Oncostatin M promotes bone formation independently of resorption when signaling through leukemia inhibitory factor receptor in mice

Emma C. Walker,[1] Narelle E. McGregor,[1] Ingrid J. Poulton,[1] Melissa Solano,[1] Sueli Pompolo,[1] Tania J. Fernandes,[2] Matthew J. Constable,[2] Geoff C. Nicholson,[2] Jian-Guo Zhang,[3] Nicos A. Nicola,[3] Matthew T. Gillespie,[1,4] T. John Martin,[1,4] and Natalie A. Sims[1,4]

[1]St. Vincent's Institute, Melbourne, Victoria, Australia. [2]The Department of Clinical and Biomedical Sciences: Barwon Health, The University of Melbourne and Barwon Biomedical Research, Geelong, Victoria, Australia. [3]The Walter and Eliza Hall Institute, Parkville, Victoria, Australia. [4]Department of Medicine at St. Vincent's Hospital, The University of Melbourne, Melbourne, Victoria, Australia.

Effective osteoporosis therapy requires agents that increase the amount and/or quality of bone. Any modification of osteoclast-mediated bone resorption by disease or drug treatment, however, elicits a parallel change in osteoblast-mediated bone formation because the processes are tightly coupled. Anabolic approaches now focus on uncoupling osteoblast action from osteoclast formation, for example, by inhibiting sclerostin, an inhibitor of bone formation that does not influence osteoclast differentiation. Here, we report that oncostatin M (OSM) is produced by osteoblasts and osteocytes in mouse bone and that it has distinct effects when acting through 2 different receptors, OSM receptor (OSMR) and leukemia inhibitory factor receptor (LIFR). Specifically, mouse OSM (mOSM) inhibited sclerostin production in a stromal cell line and in primary murine osteoblast cultures by acting through LIFR. In contrast, when acting through OSMR, mOSM stimulated RANKL production and osteoclast formation. A key role for OSMR in bone turnover was confirmed by the osteopetrotic phenotype of mice lacking OSMR. Furthermore, in contrast to the accepted model, in which mOSM acts only through OSMR, mOSM inhibited sclerostin expression in *Osmr*$^{-/-}$ osteoblasts and enhanced bone formation in vivo. These data reveal what we believe to be a novel pathway by which bone formation can be stimulated independently of bone resorption and provide new insights into OSMR and LIFR signaling that are relevant to other medical conditions, including cardiovascular and neurodegenerative diseases and cancer.

Introduction

Signaling through the shared cytokine receptor subunit glycoprotein 130 (gp130) is critical for many cell functions. Specific responses are initiated by unique receptor:ligand signaling complexes formed by initial ligand binding to a specific receptor subunit, followed by complex formation with gp130 to activate intracellular signaling (1). Human oncostatin M (hOSM) is unique among gp130-signaling cytokines in that it binds first to gp130, then forms 1 of 2 possible signaling complexes with equivalent affinity, utilizing either OSM receptor (OSMR) or leukemia inhibitory factor receptor (LIFR) (2). This bimodal signaling ability has made it difficult to define the specific effects of these 2 pathways using human cells. Nevertheless, specific OSMR signaling has been implicated in melanoma (3), glioblastoma (4), lung (5) and ovarian carcinoma (6), and breast tumor (7) pathogenesis, while LIFR signaling has been implicated in cardiovascular disease (8), neurobiology, and immunity (9). In mouse cells, hOSM binds only to the LIFR:gp130 complex, while mouse OSM (mOSM) binds first to gp130 and then forms a high-affinity complex only with OSMR (10). For this reason, the mouse provides an excellent model to study distinct pathways of OSM signaling through each receptor.

Signaling through gp130 is critical in bone remodeling (11), a system dependent on intercellular communication among osteoclasts (bone-resorbing cells), osteoblasts (bone-forming cells), and osteocytes (terminally differentiated osteoblast-lineage cells embedded in the bone matrix) (12). Genetic deletion of gp130 or the LIFR in mice results in a neonatal lethal phenotype that includes osteopenia due to increased osteoclast formation and reduced bone formation (13, 14), and in humans, a mutation in the LIFR is associated with early mortality and skeletal defects (15). gp130 expression by cultured osteoblast-like cells is stimulated by hormones and inflammatory cytokines known to increase bone resorption, including 1,25-dihydroxyvitamin-D_3 ($1,25D_3$), parathyroid hormone (PTH), and IL-1 (16). Furthermore, osteoclast formation is stimulated by these factors in a manner dependent, at least in part, on gp130 (17). It has been known for many years that hOSM and mOSM stimulate osteoclast formation by enhancing RANKL expression by osteoblast-lineage cells (18–21).

Osteoblasts and adipocytes are derived from common mesenchymal precursors, and hOSM and mOSM also modulate their differentiation, although interpretation of early results is complicated by species differences. hOSM has been reported either to inhibit or stimulate a bone formation–associated enzyme, alkaline phosphatase (ALP), in mouse primary osteoblasts (22) and murine stromal cells (23), respectively. Adenoviral transfer of mOSM to a mouse arthritis model stimulated bone formation (24), and administration of hOSM to human adipose–derived mesenchymal stem cells promoted ALP activity

Conflict of interest: The authors have declared that no conflict of interest exists.
Citation for this article: *J Clin Invest* doi:10.1172/JCI40568.

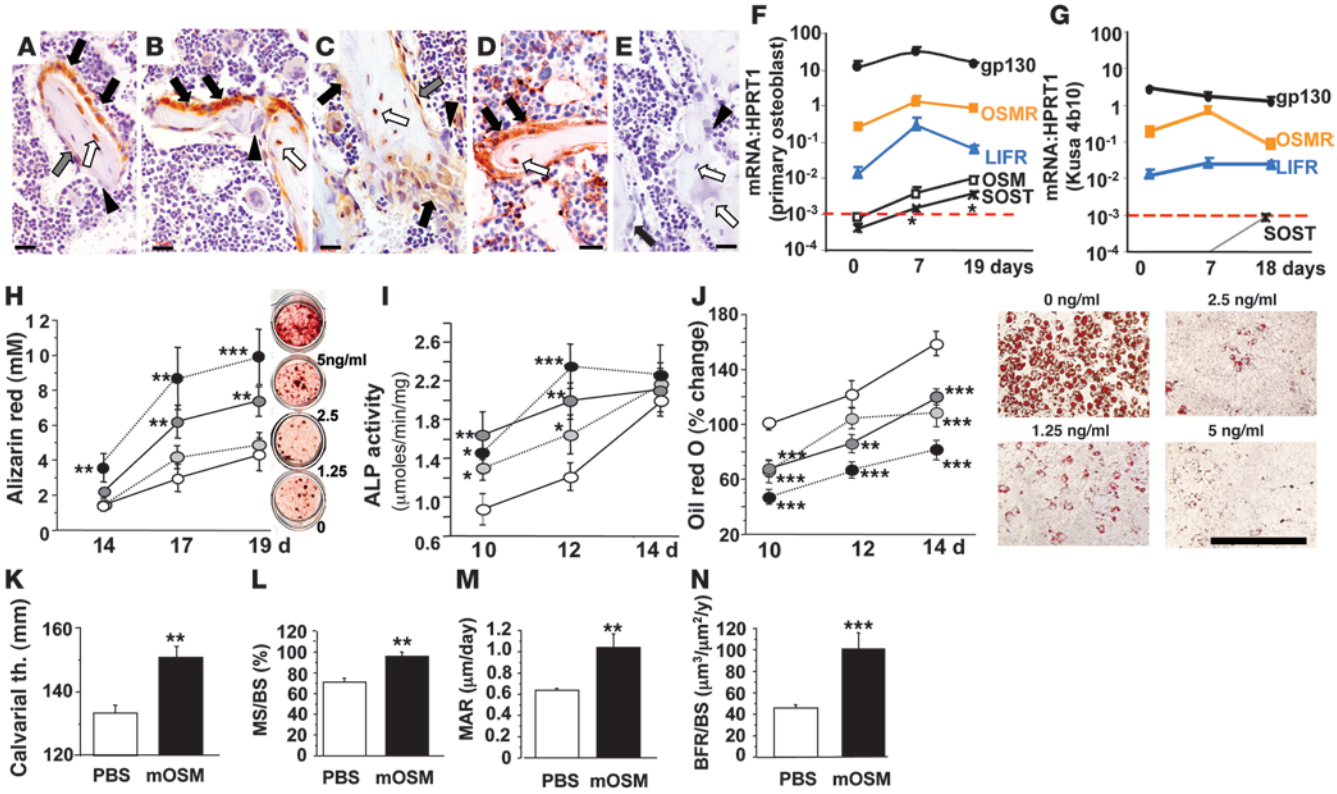

Figure 1

OSM and OSMR are expressed in osteoblasts, and OSM stimulates bone formation and inhibits adipogenesis. Immunostaining for OSM (**A** and **B**), OSMR (**C**), and LIFR (**D**) in osteoblasts (black arrows), osteocytes (white arrows), and bone-lining cells (gray arrows). No staining was observed for OSM or OSMR in osteoclasts (black arrowheads) or antibody negative control (**E**). Scale bars: 10 μm. qPCR of primary calvarial osteoblasts (**F**) and Kusa 4b10 murine stromal cells (**G**) during osteoblast differentiation confirmed mRNA transcription for OSMR, gp130, LIFR, and increasing OSM levels in calvarial osteoblasts parallel to sclerostin (SOST). Dashed line indicates lower limit of detection (Ct > 35). OSM was not detected in Kusa 4b10 cells. (**H**–**J**) Mineralization (solubilized alizarin red staining) and ALP activity were significantly increased in Kusa 4b10 cells treated with mOSM at 1.25 ng/ml (light gray), 2.5 ng/ml (dark gray), and 5 ng/ml (black) compared with vehicle-treated controls (white). Representative alizarin red staining shown for day 19 before elution. In adipogenic medium, mOSM inhibited Kusa 4b10 adipogenesis (solubilized oil red O staining); representative images shown for day 14 before elution. Scale bar: 500 μm. Data for **F**–**J** are all mean ± SEM of 3 independent experiments (triplicate wells). $^{*}P < 0.05$; $^{**}P < 0.01$; $^{***}P < 0.001$ vs. time-matched vehicle-treated cells. (**K**–**M**) Calvarial injection of 2 μg/d mOSM for 5 days in C57BL/6 mice increased calvarial thickness (Th.), MS/BS, MAR, and BFR/BS. Data are shown as mean + SEM, 6 mice/group. $^{**}P < 0.01$; $^{***}P < 0.001$ vs. saline-treated controls.

and inhibited adipocyte differentiation (25), indicating that, within species, hOSM and mOSM consistently increase osteoblast differentiation.

We sought to determine the local role of mOSM in bone by identifying OSM- and OSMR-expressing cells, the pathways by which OSM modifies osteoblast and osteoclast differentiation, and by analyzing skeletons and cultured osteoblast-lineage cells from *Osmr*$^{-/-}$ mice (26). These studies led to the discovery that, while OSMR signaling mediates the effects of mOSM on osteoclast differentiation and adipogenesis, there is at least one specific action of mOSM mediated by LIFR, and this action inhibits sclerostin and promotes bone formation without influencing osteoclast differentiation.

Results

OSM, OSMR, and LIFR are expressed by osteoblast-lineage cells. Immunohistochemistry detected OSM protein at high levels in osteoblasts at all stages of differentiation, including bone-forming osteoblasts, bone-lining cells, and osteocytes; OSM was not detected in osteoclasts (Figure 1, A and B). Adult mouse bone stained positively for OSMR and LIFR in osteoblasts, bone-lining cells, and osteocytes, but not in osteoclasts or negative control sections (Figure 1, C–E). LIFR was also detected in marrow cells, including megakaryocytes and endothelial cells, consistent with previous reports (27–29).

Osm mRNA production by the osteoblast lineage was confirmed by quantitative real-time PCR (qPCR) of cell-culture preparations from mouse calvariae (primary calvarial osteoblasts) and the murine stromal cell line Kusa 4b10 (Figure 1, F and G). Cells in both systems, under appropriate stimuli, can differentiate into adipocytes or osteoblasts (30), and when differentiated for 17 days, also express sclerostin, a specific osteocyte marker, indicating the presence of terminally differentiated osteocytes (31). During differentiation of osteoblasts from calvarial preparations, *Osm* mRNA levels increased in parallel with sclerostin (Figure 1F). OSMR, gp130, and LIFR were detected at high levels in calvarial osteoblast cultures and Kusa 4b10 cells (Figure 1, F and G), while *Osm* mRNA was not detected in Kusa 4b10 cells (Figure 1G). mRNA for gp130-like receptor (GPL), an alternative α receptor subunit

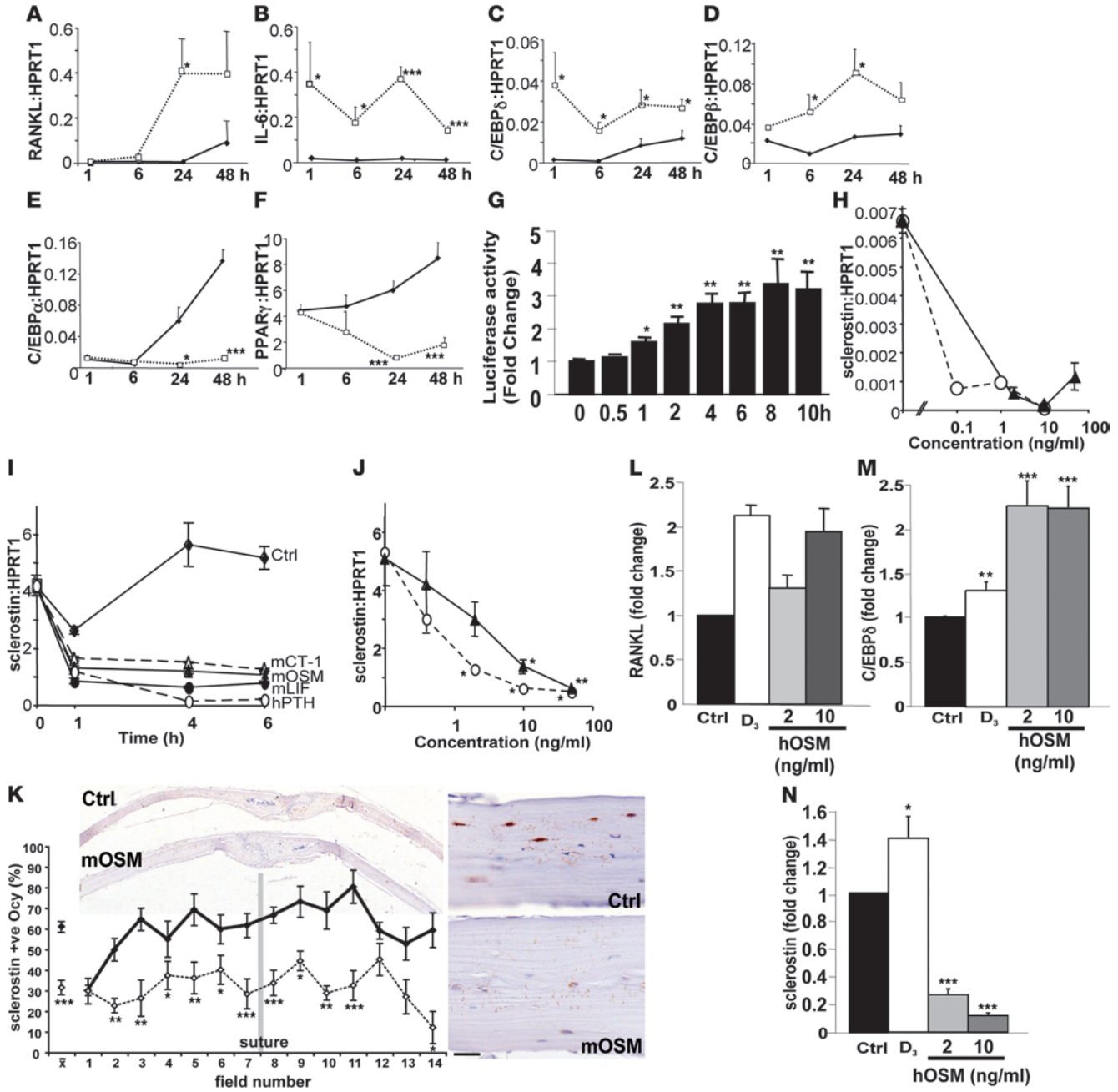

Figure 2

mOSM regulates osteoclast, osteoblast, and adipocyte target genes and inhibits sclerostin. (**A**–**F**) Effect of 10 ng/ml mOSM (dashed line) on target genes in undifferentiated Kusa 4b10 cells versus control (solid line). (**G**) 10 ng/ml mOSM increased 6×OSE2 luciferase activity in UMR106-01 cells. **A**–**G** show mean ± SEM from 3 independent experiments. *$P < 0.05$; **$P < 0.01$; ***$P < 0.001$ vs. control or time zero. (**H**) Treatment of 17-day differentiated primary calvarial osteoblasts with mOSM (solid) or $hPTH_{1–34}$ (dashed) inhibited sclerostin mRNA. (**I**) mOSM (50 ng/ml), mLIF (50 ng/ml), mCT-1 (50 ng/ml), or $hPTH_{1–34}$ (10 ng/ml) all reduced sclerostin mRNA:HPRT1 in UMR 106-01 cells. **H** and **I** show mean ± SD of a representative of 3 experiments with similar results. (**J**) Treatment of UMR 106-01 cells with mOSM (solid) or $hPTH_{1–34}$ (dashed) for 8 hours inhibited sclerostin mRNA. Data shown are mean ± SEM of 3 experiments. *$P < 0.05$; **$P < 0.01$ vs. control. (**K**) Reduced percentage of sclerostin-positive (+ve) osteocytes (Ocy) in calvariae of C57BL/6 mice after treatment with 2 μg/d mOSM (dashed line) compared with vehicle (solid line). High-power images show typical regions. Scale bar: 10 μm. Data are shown as mean ± SEM, $n = 8$ per group. x indicates mean of entire calvariae; 1–15 are each 380-μm wide fields across the calvaria, shown aligned with low-power images. *$P < 0.05$; **$P < 0.01$; ***$P < 0.001$ vs. control. (**L**–**N**) Effect of hOSM and $1,25D_3$ (D_3) on target genes in human osteoblasts from 3 donors (2 for RANKL). Data are shown as mean + SEM (SD for RANKL). *$P < 0.05$; **$P < 0.01$; ***$P < 0.001$ vs. control (Ctrl).

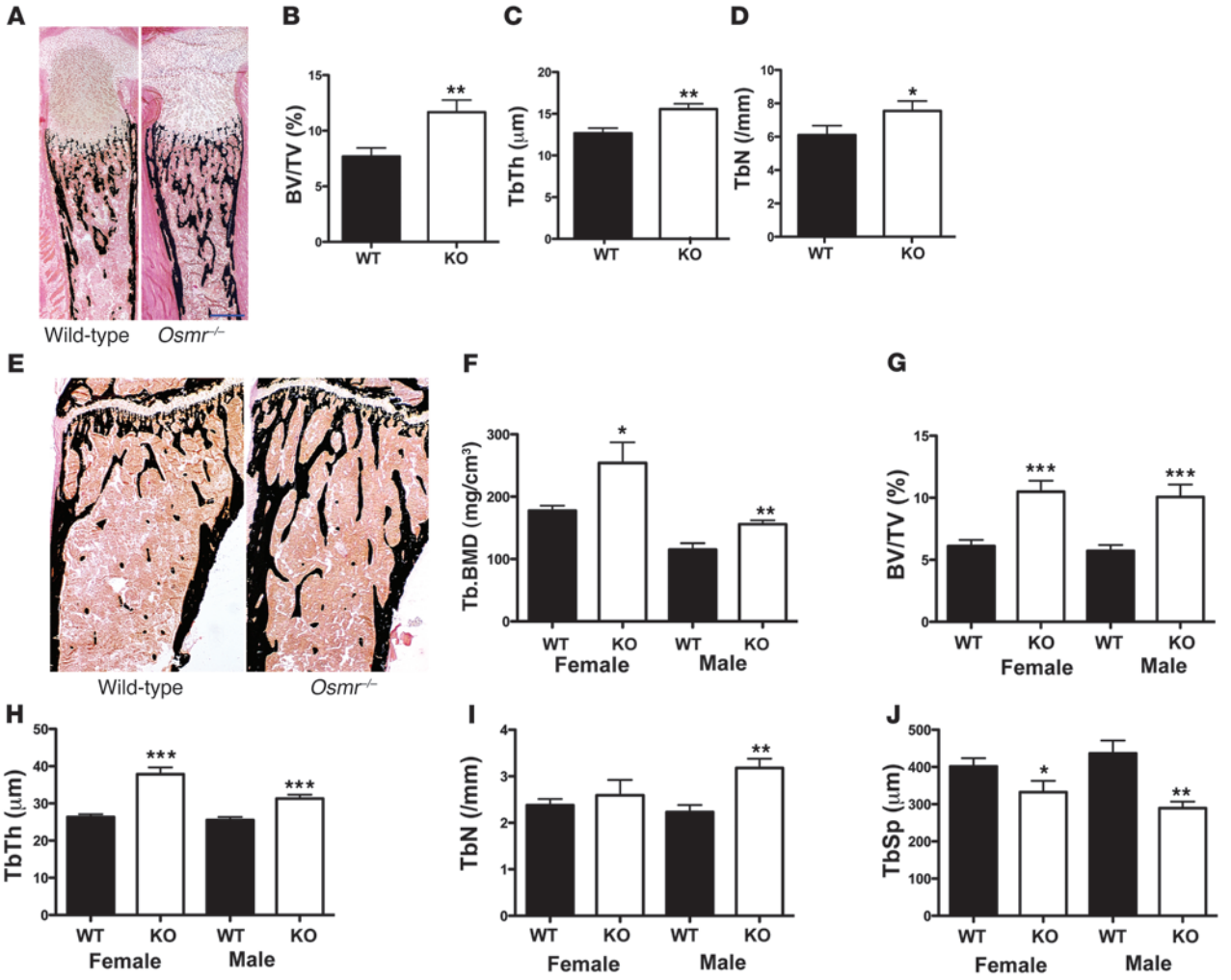

Figure 3

Increased trabecular bone mass in *Osmr*$^{-/-}$ mice. Representative images from 1-day-old WT and *Osmr*$^{-/-}$ littermate tibiae (**A**) stained by a modified von Kossa method (bone stains black) showing normal size and no reduction in trabecular bone. Scale bar: 250 μm. BV/TV (**B**), TbTh (**C**), and TbN (**D**) were all increased in neonate *Osmr*$^{-/-}$ tibiae compared with WT. Data are shown as mean + SEM, $n = 6$ mice/group. $^{*}P < 0.05$; $^{**}P < 0.01$ vs. WT littermates. Von Kossa–stained tibiae from representative 12-week-old female WT and *Osmr*$^{-/-}$ mice (**E**). Scale bar: 250 μm. Tb.BMD was significantly increased in female and male *Osmr*$^{-/-}$ femora at 12 weeks of age compared with age- and strain-matched WT controls (**F**). (**G**–**J**) BV/TV, TbTh, TbN, and TbSp in male and female 12-week-old *Osmr*$^{-/-}$ mice and WT controls. Data are shown as mean ± SEM, $n = 8$–12 mice per group. $^{*}P < 0.05$; $^{**}P < 0.01$; $^{***}P < 0.001$ vs. WT littermates.

that binds OSMR and responds to IL-31 (32), was not detectable in either primary calvarial osteoblasts or Kusa 4b10 cells, confirming that mOSM is the only ligand capable of signaling through OSMR expressed by murine osteoblasts.

mOSM stimulates bone formation and inhibits adipogenesis. Previous studies of OSM in osteoblasts have been complicated by mixed use of mOSM and hOSM in non–species-matched cells (22, 23); the effect of mOSM in murine stromal cells has not been reported. Since primary calvarial osteoblasts contain a mixed population of cells, we used Kusa 4b10 cells to assess this. mOSM treatment dose dependently increased mineralization and ALP activity of Kusa 4b10 cells (Figure 1, H and I) and dramatically impaired adipogenesis (Figure 1J). Both effects were similar to what occurred in previous observations for mouse cardiotrophin-1 (mCT-1), mLIF, and mIL-11 (33). IL-31 had no effect on mineralization, ALP activity, or adipogenesis (data not shown).

The ability of mOSM to stimulate bone formation was then assessed by injecting mOSM over calvariae of 5-week-old male C57BL/6 mice. Calvarial thickness, mineral apposition rate (MAR), mineralizing surface/bone surface (MS/BS), and bone formation rate/BS (BFR/BS) were all significantly increased by mOSM treatment (Figure 1, K–N). Thus, in addition to its role in stimulating the osteoblast to support osteoclast differentiation, mOSM enhances bone formation.

mOSM inhibits sclerostin and modifies other genes associated with osteoblast, osteocyte, and adipocyte differentiation. In Kusa 4b10 stromal cells, mOSM increased mRNA levels of key osteoclastogenic genes, *Rankl* and *Il6*, rapidly induced osteoblast transcription factors CCAAT-enhancer binding protein δ (C/EBPδ) and C/EBPβ, and inhibited the adipocytic factors PPARγ and C/EBPα (Figure 2, A–F). In Kusa 4b10 cells differentiated to form osteoblasts and osteocytes, mRNA levels for *Cebpa* and *Pparg* were not reduced by mOSM, but *Rankl*,

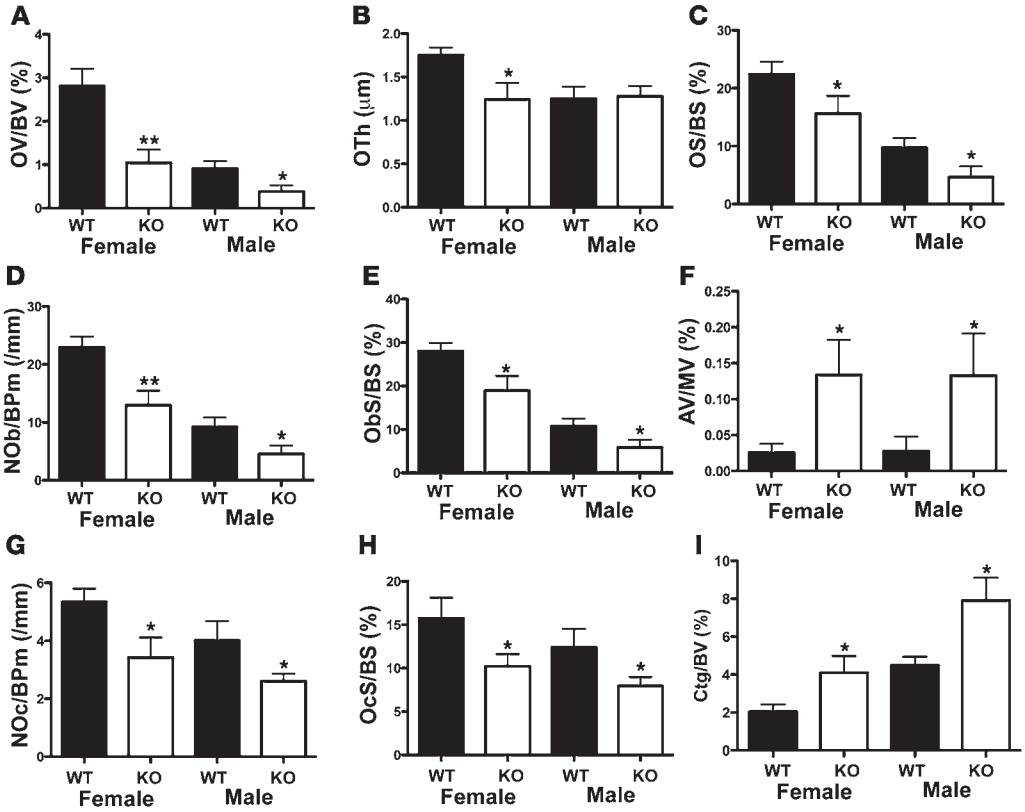

Figure 4
Osmr$^{-/-}$ mice have reduced bone remodeling and increased adipogenesis. Bone formation (**A**–**E**), marrow adipogenesis (**F**), and bone resorption (**G**–**I**) parameters in 12-week-old male and female *Osmr*$^{-/-}$ proximal tibiae. OV/BV, OTh, OS/BS, NOb/BPm, and ObS/BS were reduced in 12-week-old female and male *Osmr*$^{-/-}$ mice compared with WT littermates. Marrow adipocyte volume (AV/MV) was significantly increased in male and female 12-week-old *Osmr*$^{-/-}$ mice compared with WT mice. NOc/BPm and OcS/BS were significantly reduced in 12-week-old male and female *Osmr*$^{-/-}$ mice, and CtgV/BV was elevated, confirming a reduction in bone resorption. Data are shown as mean + SEM. $^{*}P < 0.05$; $^{**}P < 0.01$ vs. WT littermates. n = 8–10 per group.

Il6, *Cebpd*, and *Cebpb* mRNA levels were all increased (Supplemental Table 1; supplemental material available online with this article; doi:10.1172/JCI40568DS1). Consistent with runx2 activation by C/EBPδ, mOSM also activated transcription of a 6×OSE2 reporter construct (Figure 2G). In addition, the osteocyte-derived mineralization inhibitor, sclerostin, was reduced in OSM-treated Kusa 4b10 osteoblast/osteocyte cultures (Supplemental Table 1).

Inhibition of sclerostin by mOSM was investigated further in primary calvarial osteoblasts differentiated for 17 days, at which point sclerostin is readily detected (31). Sclerostin mRNA levels were strongly inhibited by mOSM (Figure 2H) by a magnitude similar to that observed with human $PTH_{1–34}$ ($hPTH_{1–34}$), the only currently available anabolic agent for bone. This was also observed in osteocyte-like UMR 106-01 cells, which express high levels of sclerostin (Figure 2I), and a similar reduction in sclerostin mRNA levels was observed with mLIF and mCT-1, which signal through gp130:LIFR. Again, the inhibition was similar to that previously reported for $hPTH_{1–34}$ (34). mOSM and $hPTH_{1–34}$ both decreased sclerostin mRNA levels in a dose-dependent manner (Figure 2J).

Since mOSM treatment increased bone formation when administered over calvariae of WT mice (Figure 1, K–N), we used immunohistochemistry to detect sclerostin in calvariae of mOSM-treated mice, 24 hours after the fifth injection of mOSM or saline. It was evident on examination by light microscopy that the proportion of sclerostin-positive osteocytes across the mOSM-treated calvariae was reduced. When quantified, the mean percentage of sclerostin-positive osteocytes was dramatically lower with mOSM treatment (Figure 2K). To determine whether this was restricted to a particular region, a field-by-field analysis was carried out, revealing a consistent reduction in sclerostin-positive osteocytes across the entire section.

Sclerostin inhibition by OSM was also observed in human primary osteoblast/osteocyte cultures differentiated for 14 days until sclerostin was readily detectable. hOSM increased C/EBPδ and RANKL (Figure 2, L and M) and reduced sclerostin mRNA levels (Figure 2N), confirming that sclerostin inhibition by OSM is not unique to the mouse.

OSMR deletion leads to defects in bone resorption, bone formation, and adipogenesis. Neonate *Osmr*$^{-/-}$ tibiae were analyzed to allow direct comparison with the gp130 and LIFR knockouts, which are neonatal lethal (13, 14). In contrast with dwarfism and osteopenia reported in gp130 and LIFR knockouts, neonate *Osmr*$^{-/-}$ skeletons were of normal size, with increased trabecular bone volume (BV/TV), trabecular thickness (TbTh), and trabecular number (TbN) (Figure 3, A–D). No difference in osteoblast surface (ObS) or osteoclast surface (OcS) was detected: mean ObS/BS (percentage ± SEM) WT: 34.3 ± 1.9; *Osmr*$^{-/-}$: 37.3 ± 3.2, $P > 0.05$ vs. WT; mean OcS/BS (percentage) WT: 11.3 ± 1.1; *Osmr*$^{-/-}$: 11.6 ± 1.3; $P > 0.05$ vs. WT.

The increase in trabecular bone in *Osmr*$^{-/-}$ mice was maintained to adulthood (Figure 3E); trabecular bone mineral density (Tb.BMD) was significantly elevated in male and female *Osmr*$^{-/-}$ femora at 12 weeks of age (Figure 3F); cortical thickness and periosteal circumference were also increased in the metaphysis in male and female *Osmr*$^{-/-}$ mice, a mild Erlenmeyer flask morphology consistent with osteopetrosis (Supplemental Table 2). Histomorphometry confirmed this; in male and female *Osmr*$^{-/-}$ tibiae, BV/TV and TbTh were high, and TbN was increased in *Osmr*$^{-/-}$ males (Figure 3, G–I). Trabecular separation (TbSp) was reduced (Figure 3J). BV/TV was also increased in male and female vertebrae (Supplemental Table 2). *Osmr*$^{-/-}$ mice also demonstrated reduced bone formation, indicated by osteoid volume (OV/BV), osteoid thickness (OTh), osteoid surface/BS (OS/BS), ObS/BS, and osteoblast numbers/bone perimeter

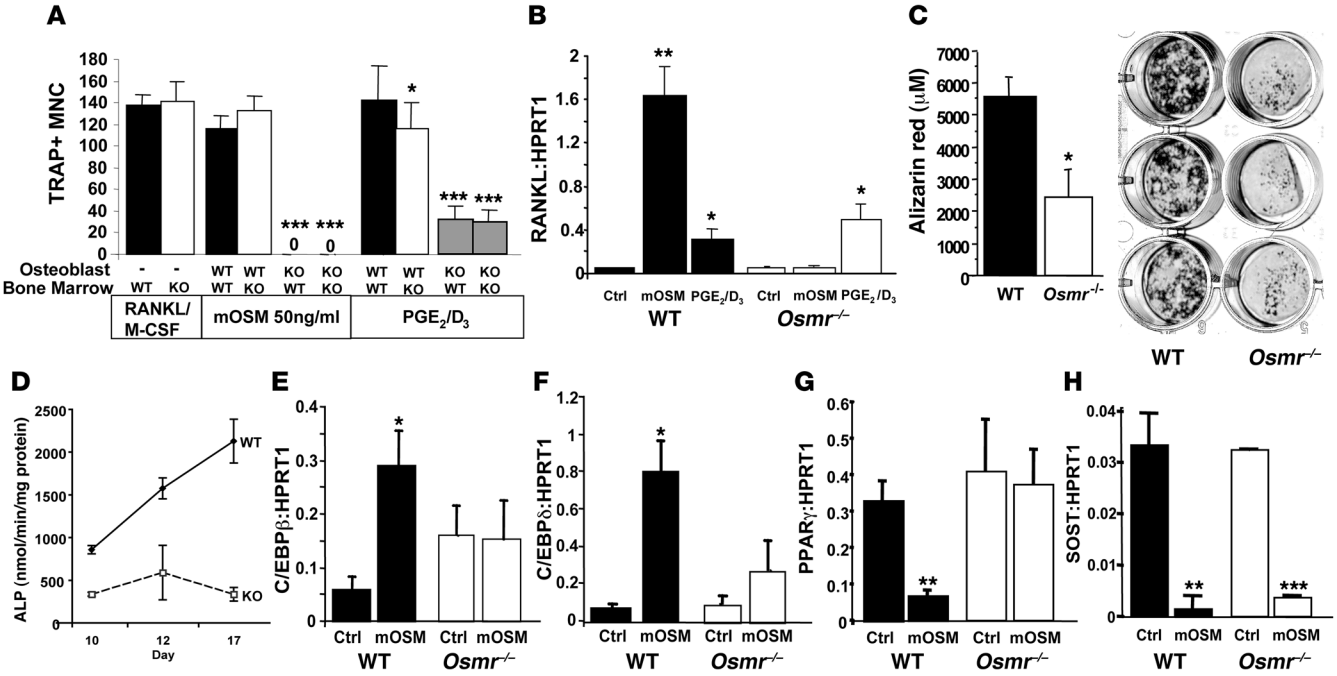

Figure 5

OSMR expression by osteoblasts is required for normal osteoclast and osteoblast activity; sclerostin is regulated by mOSM in *Osmr*$^{-/-}$ mice. (**A**) Tartrate-resistant acid phosphatase–positive multinucleated osteoclast-like cell (TRAP+ MNC) formation in response to RANKL from *Osmr*$^{-/-}$ BM macrophages compared with WT BM. In the presence of *Osmr*$^{-/-}$ osteoblasts, osteoclast formation from either *Osmr*$^{-/-}$ or WT BM in response to mOSM was completely blocked, and osteoclast formation in response to PGE_2 and $1,25D_3$ (PGE_2/D_3) was inhibited. (**B**) *Rankl* mRNA was increased by mOSM treatment in WT calvarial osteoblasts, but not in *Osmr*$^{-/-}$ calvarial osteoblasts. *Rankl* mRNA levels were also significantly increased by PGE_2/D_3 in both WT and *Osmr*$^{-/-}$ primary calvarial osteoblasts 8 hours after treatment was commenced. (**C** and **D**) Mineralization, measured by alizarin red staining after 21 days of culture in mineralizing medium, and ALP activity in cells grown in osteoblast differentiation medium were both significantly reduced in calvarial osteoblasts generated from *Osmr*$^{-/-}$ mice compared with WT littermates. (**E**–**H**) *Cebpb*, *Cebpd*, *Pparg*, and *Sost* mRNA levels, relative to HPRT1 in WT and *Osmr*$^{-/-}$ calvarial osteoblasts after treatment with 10 ng/ml mOSM. PPARγ and SOST are measured in cells differentiated for 17 days in osteoblast differentiation medium. All data in Figure 5 are shown as mean + SEM from 3–4 independent experiments, carried out in triplicate. **P* < 0.05; ***P* < 0.01; ****P* < 0.001 vs. untreated control at the same time point.

(NOb/BPm) (Figure 4, A–E). In contrast, marrow adipocyte volume was significantly increased (Figure 4F). Consistent with an osteopetrotic phenotype, OcS/BS and osteoclast numbers/BPm (NOc/BPm) were significantly reduced (Figure 4, G and H). A reduction in bone resorption was confirmed by an increase in cartilage volume within the trabecular bone (CtgV/BV) (Figure 4I). Despite the low number of osteoblasts and low osteoid, MAR was not significantly altered in either male or female tibiae (data not shown), and MS/BS and BFR/BS were mildly increased in the tibiae of female mice only (males not shown; female mean MS/BS [percentage ± SEM] WT: 28.1 ± 2.3 knockout: 34.9 ± 2.4, $P = 0.035$ vs. WT; mean BFR/BS [$mm^2/mm^3/y$] WT: 182 ± 22 knockout: 254 ± 22, $P = 0.021$ vs. WT). This increase in MS/BS (a component of BFR/BS) may have been caused by reduced calcein label resorption due to the reduced osteoclast generation. In vertebrae, MAR was significantly reduced in male and female mice (Supplemental Table 2).

Formation of osteoclasts by treatment of BM from *Osmr*$^{-/-}$ mice with RANKL and M-CSF was not significantly different from that from WT BM (Figure 5A), indicating no intrinsic defect in *Osmr*$^{-/-}$ osteoclast progenitors. When *Osmr*$^{-/-}$ osteoblasts were used as a source of osteoclastogenic factors, however, osteoclast formation was reduced in these cocultures (Figure 5A). mOSM treatment could not induce osteoclast formation in the presence of *Osmr*$^{-/-}$ osteoblasts (Figure 5A) due to blockade of the RANKL response to mOSM (Figure 5B). This confirmed that mOSM signals through OSMR to induce osteoclast formation in a RANKL-dependent manner. Furthermore, when osteoclast formation was induced by a standard strong stimulus, $PGE_2/1,25D_3$, osteoclast formation was approximately 50% of that in WT cultures, indicating that OSMR signaling is required for this stimulus to be fully effective (Figure 5A), consistent with our previous observations using a gp130-neutralizing antibody (17). Surprisingly, the induction of RANKL by $PGE_2/1,25D_3$ was not modified in *Osmr*$^{-/-}$ osteoblasts (Figure 5B), indicating that OSMR signaling may induce an osteoclast stimulus that acts independently of RANKL or may repress an osteoclast inhibitor. IL-31, which also signals through a gp130:OSMR heterodimer, did not stimulate osteoclast formation by *Osmr*$^{-/-}$ or WT BM (data not shown).

Reduced mineralized nodule formation and lower ALP activity of *Osmr*$^{-/-}$ primary calvarial osteoblasts indicated an intrinsic defect in osteoblast differentiation (Figure 5, C and D). Basal mRNA levels of osterix, ALP, and runx2 were not significantly different in *Osmr*$^{-/-}$ cells compared with WT cells, nor was there a significant difference in mRNA levels of OSM, LIF, LIFR, gp130, C/EBPδ, RANKL, osteoprotegerin (OPG), M-CSF, PPARγ, or IL-6 in *Osmr*$^{-/-}$ cells compared with WT cells (data not shown). There was a mildly higher level of sclerostin mRNA in *Osmr*$^{-/-}$ calvarial osteoblasts, but this did not reach statistical significance (data

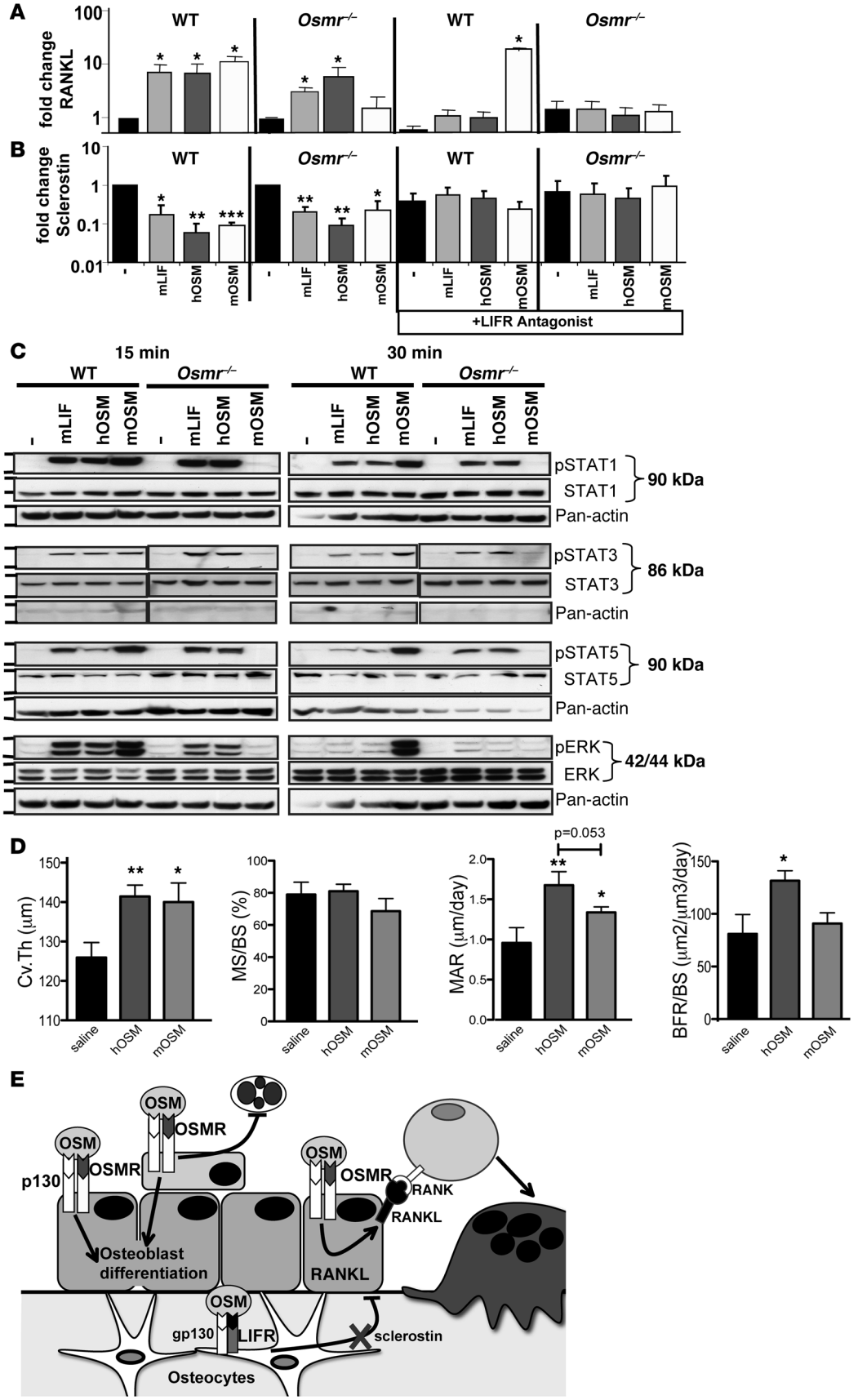
A
fold change RANKL
WT
Osmr-/-
WT
Osmr-/-
B
fold change Sclerostin
- mLIF hOSM mOSM
+LIFR Antagonist
C
15 min
30 min
pSTAT1
STAT1
90 kDa
Pan-actin
pSTAT3
STAT3
86 kDa
pSTAT5
STAT5
90 kDa
pERK
ERK
42/44 kDa
D
Cv.Th (μm)
MS/BS (%)
MAR (μm/day)
p=0.053
BFR/BS (μm2/μm3/day)
saline
hOSM
mOSM
E
OSM
OSMR
p130
Osteoblast differentiation
RANK
RANKL
gp130
LIFR
sclerostin
Osteocytes

Figure 6
mOSM stimulates RANKL via OSMR yet inhibits sclerostin via LIFR and stimulates bone formation in *Osmr*$^{-/-}$ mice. (**A** and **B**) Fold changes in *Rankl* and *Sost* mRNA levels in primary calvarial osteoblasts 6 hours after commencing treatment with mLIF, hOSM, or mOSM (all 2 ng/ml) with and without 1 hour pretreatment with 2.5 μg/ml LA. Mean ± SEM of 3 independent experiments. **P* < 0.05; ***P* < 0.01; ****P* < 0.001 vs. vehicle-treated cells of the same genotype and antagonist exposure. (**C**) Phosphorylation of WT and *Osmr*$^{-/-}$ osteoblasts stimulated with mLIF, hOSM, or mOSM (each 50 ng/ml). pSTAT1/STAT1 (90 kDa), pSTAT3/STAT3 (86 kDa), pSTAT5/STAT5 (90 kDa) detected between 98 kDa and 62 kDa molecular weight markers (left side of figure). pERK/ERK (42/44 kDa) and pan-actin (42 kDa) were detected between 49 kDa and 38 kDa. The pSTAT3/STAT3 Western blot is from 1 film, but it has been spliced to maintain a consistent order within the figure. pSTAT1/STAT1 and pERK/ERK were probed sequentially on the same gel. (**D**) hOSM and mOSM (both 2 ng/ml) injected over calvariae of *Osmr*$^{-/-}$ mice (n = 5–6/group) increased calvarial thickness (Cv.Th.) without increasing MS/BS, but increased MAR, and hOSM increased BFR/BS compared with saline-treated controls. **P* < 0.05; ***P* < 0.01, vs. saline-treated control. (**E**) A model of mOSM action. OSM, produced by osteoblasts, osteocytes, and bone-lining cells acts through OSMR in osteoblasts and their precursors to promote osteoblast differentiation and inhibit adipocyte differentiation as well as stimulating osteoclast differentiation by increasing RANKL expression. In contrast, in the osteocyte, mOSM acts through LIFR in osteocytes to inhibit sclerostin, an osteocyte-specific inhibitor of mineralization, thus modifying bone formation independently of effects on osteoclast and adipocyte differentiation.

not shown). Consistent with original observations in other tissues (26), *OSMR* mRNA was undetectable in *Osmr*$^{-/-}$ calvarial osteoblast cultures. In *Osmr*$^{-/-}$ mice, OSM was detected by immunohistochemistry at normal distribution and OSMR was not detected (Supplemental Figure 1). mRNA levels for sclerostin and RANKL were not significantly altered in mRNA extracted from femora of 9-week-old *Osmr*$^{-/-}$ mice compared with WT littermates (data not shown).

To assess whether mOSM could modify gene targets associated with osteoblast and adipocyte differentiation in the absence of OSMR, WT and *Osmr*$^{-/-}$ primary calvarial osteoblasts were treated with mOSM. As observed with RANKL, mOSM effects on *Cebpd*, *Cebpb*, and *Pparg* mRNA levels were ablated in the absence of OSMR (Figure 5, E–G). Surprisingly, however, sclerostin repression by mOSM remained fully effective in *Osmr*$^{-/-}$ calvarial cultures (Figure 5H).

We hypothesized that mOSM may inhibit sclerostin through LIFR. Since LIFR-null mice have a neonatal lethal defect, this possibility was assessed by treating sclerostin-expressing *Osmr*$^{-/-}$ and WT primary calvarial cultures with a LIFR antagonist (LA) prior to mLIF, hOSM, or mOSM treatment. LA is a modified form of hLIF with enhanced binding to LIFR that is unable to activate gp130 or bind OSMR (35). The ability of LA to block LIFR signaling in our culture system was confirmed by blockade of the increase in RANKL induced by mLIF and hOSM in both WT and *Osmr*$^{-/-}$ cultures (Figure 6A). LA did not prevent the increase in *Rankl* mRNA levels induced by mOSM in WT cells, further confirming specificity for LIFR. In contrast, mLIF-, hOSM-, and mOSM-induced reductions in sclerostin mRNA were all ablated by LA in WT osteoblasts, indicating that these effects are mediated by LIFR (Figure 6B). Furthermore, the reduction in sclerostin mRNA induced by mLIF, hOSM, and mOSM in *Osmr*$^{-/-}$ mice was also ablated by LA. This indicates that, in both WT and *Osmr*$^{-/-}$ osteoblasts, LIFR mediates the reduction in sclerostin mRNA levels induced, not only by mLIF and hOSM, but also by mOSM.

To determine possible intracellular mediators of the effect of mOSM on sclerostin expression in *Osmr*$^{-/-}$ cells, we carried out Western blot analysis on WT and *Osmr*$^{-/-}$ osteoblasts treated with mLIF, hOSM, and mOSM. STAT1, STAT3, STAT5, and ERK were all phosphorylated in response to mLIF, hOSM, and mOSM in WT cells. Effects of mLIF and hOSM were unchanged in *Osmr*$^{-/-}$ cells. Phosphorylation of STAT1 and STAT5 in response to mOSM was abolished in *Osmr*$^{-/-}$ cells. In contrast, in the absence of OSMR, mOSM retained the ability to induce phosphorylation of STAT1 and ERK at very low levels 30 minutes after administration (Figure 6C).

Finally, to determine whether the LIFR-mediated inhibition of sclerostin by mOSM in the absence of OSMR may be sufficient to stimulate bone formation, we injected mOSM over the calvariae of *Osmr*$^{-/-}$ mice, using hOSM as a positive control. mOSM significantly increased calvarial thickness and MAR in *Osmr*$^{-/-}$ mice (Figure 6D). Similar effects were observed with hOSM, with the exception that hOSM also increased BFR (Figure 6D). This indicates that mOSM inhibits sclerostin and stimulates bone formation independently of OSMR, indicating what we believe is a novel LIFR-dependent pathway through which bone formation may be stimulated without effects on RANKL and osteoclast differentiation.

Discussion

OSM has been known for many years as an activated T cell product that potently stimulates bone resorption in vitro (18–21), suggesting a role in skeletal conditions in which inflammation is known to play a role, including rheumatoid arthritis (36). We show here that OSM is also expressed within the osteoblast lineage and acts locally to stimulate both bone formation and resorption by actions within this lineage. Increased bone mass in neonate and adult mice lacking OSMR confirmed a requirement for OSM in normal skeletal development and bone remodeling. Specifically, low bone formation and low bone resorption were observed, with impaired osteoclast formation dominating such that bone mass was increased. Both defects appeared to be contained within the osteoblast lineage; *Osmr*$^{-/-}$ osteoblasts demonstrated impaired ALP activity, mineralized nodule formation, and impaired support of osteoclastogenesis in vitro. Furthermore, while mOSM stimulated osteoclast formation through osteoblastic OSMR signaling, mOSM stimulated mineralization in vivo and inhibited sclerostin transcription through LIFR. A low-affinity binding of mOSM to the LIFR has been reported (10), and we now show that this produces a biologically relevant effect, specifically modifying bone formation without acting on osteoclasts. While these findings have been made in the mouse, they provide a framework to explore the possibility that separate signaling pathways could operate in human cells. This provides what we believe is a novel approach by which bone formation can be stimulated without modifying osteoclast formation, unlike the current anabolic therapy, PTH (37). As a related implication, the possibility that mOSM:gp130:LIFR signals within the cell in a manner distinct from LIF:gp130:LIFR or hOSM:gp130:LIFR (i.e., without stimulating RANKL) suggests an alternative complex conformation induced by mOSM. Another possibility is that altered levels of LIFR occupancy may activate different pathways, but we have not observed a difference in dose responses of RANKL and sclerostin induction in response to mLIF (data not shown). It should also be noted that within the calvarial osteoblast prepara-

tions, it is likely that the cells producing RANKL and sclerostin are distinct subpopulations, since *Rankl* mRNA is detected in early stages of osteoblast differentiation through to newly embedded osteocytes (38), while sclerostin is detected exclusively in mature osteocytes deeply embedded within mineralized bone.

The process of bone remodeling depends on communication among osteoclasts, osteoblasts, and osteocytes (12). Locally acting factors produced by osteoblast lineage cells, including RANKL and PTHrP, are critical for normal osteoclast and osteoblast differentiation. OSM production throughout osteoblast differentiation, including by bone-forming osteoblasts, osteocytes embedded within the bone matrix, and lining cells, and reduced bone remodeling in *Osmr*$^{-/-}$ mice, indicate that OSM is an essential stimulus of both bone resorption and formation through actions within the osteoblast lineage. Of particular interest are the production of OSM and OSMR by osteocytes and the inhibition of sclerostin expression by OSM both in vitro and in vivo. The osteocytic network within bone is only recently gaining appropriate attention (39). Osteocytes, residing within the calcified bone matrix itself, make up 90% of all bone cells, and their long processes extend through the matrix to form a communication network with osteoblasts on the bone surface. Sclerostin appears to be produced exclusively by osteocytes and inhibits bone formation (40). Sclerostin-null mice have very high bone mass, and conversely, severe bone loss occurs in transgenic mice overexpressing sclerostin in osteocytes. Human sclerostin gene mutations are responsible for sclerosteosis and van Buchem disease (41), conditions of greatly increased bone density. Recently, sclerostin antibodies have been shown to stimulate bone formation in rodent models of osteoporosis (42) and colitis-induced bone loss (43). We now show that hOSM and mOSM also rapidly inhibit sclerostin in a manner similar to that of the only approved anabolic therapy for bone, PTH (34, 44). Sclerostin inhibition by another osteocytic protein is the first evidence of regulation within this cell network. In *Osmr*$^{-/-}$ calvarial osteoblasts, mOSM did not increase expression of a number of genes associated with bone formation but did decrease expression of sclerostin. The ability of mOSM to increase calvarial thickness in *Osmr*$^{-/-}$ mice confirms that sclerostin inhibition alone can effectively increase bone formation.

Other cytokines that form a signaling complex with gp130:LIFR, mLIF and mCT-1, also inhibited sclerostin production. Since CT-1 is produced by osteoclasts (33), this suggests a novel communication pathway from the osteoclast to the osteocyte that may be involved in the coupling of bone resorption to formation, a process essential in normal bone remodeling but poorly understood. Of note, mLIF and mCT-1 are only known to form a complex with LIFR:gp130, by which they also stimulate osteoclast formation (33), so the regulation of RANKL and sclerostin through independent pathways appears unique to mOSM.

As well as inhibiting sclerostin production, OSM rapidly stimulated osteoblast differentiation while inhibiting adipocyte differentiation. mOSM acted through OSMR to downregulate PPARγ and C/EBPα while increasing mRNA levels for C/EBPδ and C/EBPβ, transcription factors that act synergistically with runx2 at OSE2 sites found in osteocalcin (45, 46), Smad6 (47), and Nell-1 (48) promoters. In the absence of OSMR signaling, mice displayed reduced NOb and increased marrow adipocyte volume, indicating a critical role for this pathway in osteoblast/adipocyte commitment. Surprisingly, however, the effects of mOSM on these gene targets were not required for mOSM to increase calvarial thickness, since only the sclerostin effect was retained in the absence of OSMR. The gene targets of mOSM are similar to those of CT-1 (33). Unlike CT-1, however, while mOSM inhibited sclerostin via LIFR, its effects on C/EBPs and therefore osteoblast/adipocyte commitment are mediated through OSMR, suggesting one effect in osteocytes and another effect early in stromal cell commitment. This could explain why mOSM increased MAR in *Osmr*$^{-/-}$ mice but did not increase MS/BS as it did in WT mice, since MS/BS is determined by osteoblast differentiation, while mineralization rate may be determined by mature osteoblast activity under the influence of osteocytic control.

Like PTH, OSM acts in 2 ways, as a stimulus of resorption and as a stimulus of bone formation. The ability of mOSM to act within the osteoblast lineage through LIFR to inhibit sclerostin expression and through OSMR to stimulate RANKL, as illustrated in Figure 6E, provides a new possibility for osteoporosis therapy. From a therapeutic perspective, a small molecule agonist to the mOSM-binding site in the LIFR could be exploited as an anabolic pathway. This will require crystallization studies to determine differences in complex formation. Since OSMR and LIFR signaling also play significant roles in melanoma (3), glioblastoma (4), lung (5) and ovarian carcinoma (6), and breast tumor (7) pathogenesis, cardiovascular disease (8), neurobiology, and immunity (9), further investigation into other specific mOSM:LIFR targets could provide useful information for treatment of many human diseases.

Methods

Animals and histology. *Osmr*$^{-/-}$ mice backcrossed onto C57BL/6 were obtained from Anne Reutens (Monash University, Melbourne, Australia) and Atsushi Miyajima (University of Tokyo, Tokyo, Japan) (26). For all studies, littermate controls were used. All animal procedures were approved by the St. Vincent's Health Melbourne Animal Ethics Committee. Histomorphometric and peripheral quantitative computer tomography (pQCT) analysis were performed as previously described (49). Immunohistochemistry was carried out as previously described (33) using 5 μg/ml of goat anti-mOSMRβ, 2.5 μg/ml of goat anti-mOSM (R&D Systems), 1.5 μg/ml goat anti-mouse sclerostin, or 20 μg/ml of rabbit anti-human LIFR (Santa Cruz Biotechnology Inc.) followed by 6 μg/ml biotinylated goat anti-goat or goat anti-rabbit IgG (DakoCytomation). Suppliers of recombinant proteins were as follows: mOSM, hOSM, and mCT-1 (R&D Systems); mLIF (Chemicon); and $hPTH_{1-34}$ (Bachem). Calvarial in vivo administration of 0.2 μg mOSM, 0.2 μg hOSM, and saline was carried out as previously described in 5-week-old WT or *Osmr*$^{-/-}$ mice (33). Samples for histomorphometry were assessed 10 days after the final injection, while samples for immunohistochemistry were collected 24 hours after the final injection.

Cell culture. Kusa 4b10 studies, qPCR, and 6×OSE2 reporter assays were carried out as previously described (33). Primary mouse calvarial osteoblasts and primary human osteoblasts were generated as previously described (50, 51). For cultures from WT and *Osmr*$^{-/-}$ mice, animals were taken from homozygous matings using cousin litters for controls. Osteoclastic potential of BM was determined as previously described (52). Osteoclasts were generated in the presence of osteoblasts using the coculture system previously described (50).

Western analysis. Primary calvarial osteoblasts were seeded at 1×10^6 cells/10 cm^2 dish (Falcon) in α-MEM plus 10% FBS until subconfluent. Cells were serum starved (α-MEM plus 2% FBS) overnight prior to treatment, then exposed to mLIF, hOSM, or mOSM before washing twice in ice-cold PBS. Total protein lysates were collected in RIPA lysis buffer containing 150 mM NaCl (Merck), 1 mM EDTA (BDH), 1% Triton X-100 (Sigma-Aldrich), 1% sodium deoxycholate (Sigma-Aldrich), 0.1% SDS (Sigma-Aldrich), and 20 mM Tris, pH 8.0 (Ameresco). Lysates were briefly sonicated

on ice and concentrations determined by bicinchoninic acid (BCA) as per the manufacturer's instructions (Pierce). Proteins were resolved on 12% gradient gel (NuPAGE; Invitrogen) and transferred using semi-dry system (Bio-Rad) prior to probing with antibodies to phospho-STAT1 (no. 9171), STAT1 (no. 9172), phospho-STAT3 (no. 9136), STAT3 (no. 9139), phospho-STAT5 (no. 9358), STAT5 (no. 9310), phospho-ERK (no. 9106), ERK (no. 9106) (all from Cell Signaling Technology) and pan-actin (MS-1295-P0; Lab Vision Corp.).

Statistics. Statistically significant differences were determined by Student's *t* test using GraphPad Prism 5.0a or 1-way ANOVA followed by Fisher's post-hoc test using StatView 4.0. A *P* value of less than 0.05 was considered significant.

Acknowledgments

We thank John Wark and Susan Kantor at the Department of Medicine, Royal Melbourne Hospital, for use of their pQCT; Atsushi Miyajima, Tokyo University, and Anne Reutens, Monash University for *Osmr*$^{-/-}$ mice; and Gerard Karsenty, Columbia University, for the 6×OSE2 construct. We also thank staff at the Bioresources Centre, St. Vincent's Health, for excellent animal care. The work was supported by National Health and Medical Research Council (NHMRC) (Australia) program grants 345401 (to N.A. Sims, M.T. Gillespie, and T.J. Martin) and 461219 (to N.A. Nicola and J.G. Zhang). N.A. Sims is supported by a NHMRC (Australia) Senior Research Fellowship.

Received for publication July 20, 2009, and accepted in revised form November 11, 2009.

Address correspondence to: Natalie A. Sims, St. Vincent's Institute, 9 Princes St., Fitzroy, Victoria 3065, Australia. Phone: 613-9288-2555; Fax: 613-9416-2676; E-mail: nsims@svi.edu.au.

Melissa Solano's and Matthew T. Gillespie's present address is: Prince Henry's Institute, Level 4, Block E, Monash Medical Centre, Clayton, Victoria, Australia.

1. Bravo J, Heath JK. Receptor recognition by gp130 cytokines. *EMBO J*. 2000;19(11):2399–2411.
2. Mosley B, et al. Dual oncostatin M (OSM) receptors. Cloning and characterization of an alternative signaling subunit conferring OSM-specific receptor activation. *J Biol Chem*. 1996;271(51):32635–32643.
3. Brown TJ, Lioubin MN, Marquardt H. Purification and characterization of cytostatic lymphokines produced by activated human T lymphocytes. Synergistic antiproliferative activity of transforming growth factor beta 1, interferon-gamma, and oncostatin M for human melanoma cells. *J Immunol*. 1987;139(9):2977–2983.
4. Halfter H, Lotfi R, Westermann R, Young P, Ringelstein EB, Stogbauer FT. Inhibition of growth and induction of differentiation of glioma cell lines by oncostatin M (OSM). *Growth Factors*. 1998;15(2):135–147.
5. Ganapathi MK, et al. Resistance to interleukin 6 in human non-small cell lung carcinoma cell lines: role of receptor components. *Cell Growth Differ*. 1996;7(7):923–929.
6. Savarese TM, et al. Coexpression of oncostatin M and its receptors and evidence for STAT3 activation in human ovarian carcinomas. *Cytokine*. 2002;17(6):324–334.
7. Underhill-Day N, Heath JK. Oncostatin M (OSM) cytostasis of breast tumor cells: characterization of an OSM receptor beta-specific kernel. *Cancer Res*. 2006;66(22):10891–10901.
8. Fischer P, Hilfiker-Kleiner D. Role of gp130-mediated signalling pathways in the heart and its impact on potential therapeutic aspects. *Br J Pharmacol*. 2008;153(Suppl 1):S414–S427.
9. Linker R, Gold R, Luhder F. Function of neurotrophic factors beyond the nervous system: inflammation and autoimmune demyelination. *Crit Rev Immunol*. 2009;29(1):43–68.
10. Ichihara M, Hara T, Kim H, Murate T, Miyajima A. Oncostatin M and leukemia inhibitory factor do not use the same functional receptor in mice. *Blood*. 1997;90(1):165–173.
11. Sims NA. gp130 signaling in bone cell biology: Multiple roles revealed by analysis of genetically altered mice. *Mol Cell Endocrinol*. 2009;310(1–2):30–39.
12. Sims NA, Gooi JH. Bone remodeling: Multiple cellular interactions required for coupling of bone formation and resorption. *Semin Cell Dev Biol*. 2008;19(5):444–451.
13. Ware CB, et al. Targeted disruption of the low-affinity leukemia inhibitory factor receptor gene causes placental, skeletal, neural and metabolic defects and results in perinatal death. *Development*. 1995;121(5):1283–1299.
14. Shin HI, et al. Gp130-mediated signaling is necessary for normal osteoblastic function in vivo and in vitro. *Endocrinology*. 2004;145(3):1376–1385.
15. Dagoneau N, et al. Null leukemia inhibitory factor receptor (LIFR) mutations in Stuve-Wiedemann/Schwartz-Jampel type 2 syndrome. *Am J Hum Genet*. 2004;74(2):298–305.
16. Lin SC, et al. Regulation of the gp80 and gp130 subunits of the IL-6 receptor by sex steroids in the murine bone marrow. *J Clin Invest*. 1997;100(8):1980–1990.
17. Romas E, et al. The role of gp130-mediated signals in osteoclast development: regulation of interleukin 11 production by osteoblasts and distribution of its receptor in bone marrow cultures. *J Exp Med*. 1996;183(6):2581–2591.
18. Tamura T, et al. Soluble interleukin-6 receptor triggers osteoclast formation by interleukin 6. *Proc Natl Acad Sci U S A*. 1993;90(24):11924–11928.
19. Richards CD, Langdon C, Deschamps P, Pennica D, Shaughnessy SG. Stimulation of osteoclast differentiation in vitro by mouse oncostatin M, leukaemia inhibitory factor, cardiotrophin-1 and interleukin 6: synergy with dexamethasone. *Cytokine*. 2000;12(6):613–621.
20. Suda T, Udagawa N, Nakamura I, Miyaura C, Takahashi N. Modulation of osteoclast differentiation by local factors. *Bone*. 1995;17(2 Suppl):87S–91S.
21. Palmqvist P, Persson E, Conaway HH, Lerner UH. IL-6, leukemia inhibitory factor, and oncostatin M stimulate bone resorption and regulate the expression of receptor activator of NF-kappa B ligand, osteoprotegerin, and receptor activator of NF-kappa B in mouse calvariae. *J Immunol*. 2002;169(6):3353–3362.
22. Jay PR, Centrella M, Lorenzo J, Bruce AG, Horowitz MC. Oncostatin-M: a new bone active cytokine that activates osteoblasts and inhibits bone resorption. *Endocrinology*. 1996;137(4):1151–1158.
23. Gimble JM, et al. Regulation of bone marrow stromal cell differentiation by cytokines whose receptors share the gp130 protein. *J Cell Biochem*. 1994;54(1):122–133.
24. de Hooge AS, et al. Adenoviral transfer of murine oncostatin M elicits periosteal bone apposition in knee joints of mice, despite synovial inflammation and up-regulated expression of interleukin-6 and receptor activator of nuclear factor-kappa B ligand. *Am J Pathol*. 2002;160(5):1733–1743.
25. Song HY, Jeon ES, Kim JI, Jung JS, Kim JH. Oncostatin M promotes osteogenesis and suppresses adipogenic differentiation of human adipose tissue-derived mesenchymal stem cells. *J Cell Biochem*. 2007;101(5):1238–1251.
26. Tanaka M, Hirabayashi Y, Sekiguchi T, Inoue T, Katsuki M, Miyajima A. Targeted disruption of oncostatin M receptor results in altered hematopoiesis. *Blood*. 2003;102(9):3154–3162.
27. Allan EH, et al. Osteoblasts display receptors for and responses to leukemia-inhibitory factor. *J Cell Physiol*. 1990;145(1):110–119.
28. Hilton DJ, Nicola NA, Metcalf D. Distribution and comparison of receptors for leukemia inhibitory factor on murine hemopoietic and hepatic cells. *J Cell Physiol*. 1991;146(2):207–215.
29. Hilton DJ, Nicola N, Metcalf D. Distribution and binding properties of receptors for leukaemia inhibitory factor. *Ciba Found Symp*. 1992;167:227–239; discussion 239–244.
30. Allan EH, et al. Differentiation potential of a mouse bone marrow stromal cell line. *J Cell Biochem*. 2003;90(1):158–169.
31. Allan EH, et al. EphrinB2 regulation by PTH and PTHrP revealed by molecular profiling in differentiating osteoblasts. *J Bone Miner Res*. 2008;23(8):1170–1181.
32. Dillon SR, Sprecher C, Hammond A, Bilsborough J, Rosenfeld-Franklin M, Presnell SR, Haugen HS, Maurer M, Harder B, Johnston J, et al. Interleukin 31, a cytokine produced by activated T cells, induces dermatitis in mice. *Nat Immunol*. 2004;5(7):752–760.
33. Walker EC, et al. Cardiotrophin-1 is an osteoclast-derived stimulus of bone formation required for normal bone remodeling. *J Bone Miner Res*. 2008;23(12):2025–2032.
34. Keller H, Kneissel M. SOST is a target gene for PTH in bone. *Bone*. 2005;37(2):148–158.
35. Fairlie WD, et al. Affinity maturation of leukemia inhibitory factor and conversion to potent antagonists of signaling. *J Biol Chem*. 2004;279(3):2125–2134.
36. Langdon C, Kerr C, Hassen M, Hara T, Arsenault AL, Richards CD. Murine oncostatin M stimulates mouse synovial fibroblasts in vitro and induces inflammation and destruction in mouse joints in vivo. *Am J Pathol*. 2000;157(4):1187–1196.
37. Martin TJ, Sims NA. Osteoclast-derived activity in the coupling of bone formation to resorption. *Trends Mol Med*. 2005;11(2):76–81.
38. Kartsogiannis V, et al. Localization of RANKL (receptor activator of NF kappa B ligand) mRNA and protein in skeletal and extraskeletal tissues. *Bone*. 1999;25(5):525–534.
39. Bonewald LF, Johnson ML. Osteocytes, mechanosensing and Wnt signaling. *Bone*. 2008;42(4):606–615.
40. van Bezooijen RL, et al. Sclerostin is an osteocyte-expressed negative regulator of bone formation, but not a classical BMP antagonist. *J Exp Med*. 2004;199(6):805–814.

41. Balemans W, et al. Increased bone density in sclerosteosis is due to the deficiency of a novel secreted protein (SOST). *Hum Mol Genet*. 2001;10(5):537–543.
42. Li X, et al. Sclerostin antibody treatment increases bone formation, bone mass, and bone strength in a rat model of postmenopausal osteoporosis. *J Bone Miner Res*. 2009;24(4):578–588.
43. Eddleston A, et al. A short treatment with an antibody to sclerostin can inhibit bone loss in an ongoing model of colitis. *J Bone Miner Res*. 2009; 24(10):1662–1671.
44. Bellido T, et al. Chronic elevation of parathyroid hormone in mice reduces expression of sclerostin by osteocytes: a novel mechanism for hormonal control of osteoblastogenesis. *Endocrinology*. 2005; 146(11):4577–4583.
45. Gutierrez S, et al. CCAAT/enhancer-binding proteins (C/EBP) beta and delta activate osteocalcin gene transcription and synergize with Runx2 at the C/EBP element to regulate bone-specific expression. *J Biol Chem*. 2002;277(2):1316–1323.
46. Shin CS, et al. CCAAT/enhancer-binding protein delta activates the Runx2-mediated transcription of mouse osteocalcin II promoter. *J Mol Endocrinol*. 2006; 36(3):531–546.
47. Wang Q, et al. Bone morphogenetic protein 2 activates Smad6 gene transcription through bone-specific transcription factor Runx2. *J Biol Chem*. 2007; 282(14):10742–10748.
48. Truong T, Zhang X, Pathmanathan D, Soo C, Ting K. Craniosynostosis-associated gene nell-1 is regulated by runx2. *J Bone Miner Res*. 2007;22(1):7–18.
49. Sims NA, Brennan K, Spaliviero J, Handelsman DJ, Seibel MJ. Perinatal testosterone surge is required for normal adult bone size but not for normal bone remodeling. *Am J Physiol Endocrinol Metab*. 2006;290(3):E456–E462.
50. Quinn JM, et al. IL-23 inhibits osteoclastogenesis indirectly through lymphocytes and is required for the maintenance of bone mass in mice. *J Immunol*. 2008;181(8):5720–5729.
51. Gronthos S, Zannettino AC, Graves SE, Ohta S, Hay SJ, Simmons PJ. Differential cell surface expression of the STRO-1 and alkaline phosphatase antigens on discrete developmental stages in primary cultures of human bone cells. *J Bone Miner Res*. 1999;14(1):47–56.
52. Quinn JM, Whitty GA, Byrne RJ, Gillespie MT, Hamilton JA. The generation of highly enriched osteoclast-lineage cell populations. *Bone*. 2002; 30(1):164–170.